Electronic Supplementary Material (ESI) for Journal of Materials Chemistry C.

Supporting information

Excimer or Aggregate?
Near Infrared Electro- and Photoluminescence from Multimolecular Excited States of *N^C^N*-Coordinated Platinum(II) Complexes

Piotr Pander, Amit Sil, Rebecca J. Salthouse, Christopher W. Harris, Melissa T. Walden, J. A. Gareth Williams, and Fernando B. Dias

Table of contents

1. General

Materials and methods for synthesis and characterization of the compounds

Commercial chemicals were used as supplied without further purification. Reactions requiring an inert atmosphere were carried out using Schlenk-line techniques under an atmosphere of argon or nitrogen. Thin layer chromatography analysis was performed on F_{254} silica plates and visualized by UV irradiation at 254 and 365 nm. NMR spectra were recorded on a Bruker Avance-400 spectrometer (400 MHz), a Varian VNMRS-600 (600 MHz) or a Varian VNMRS-700 (700 MHz). Two-dimensional NMR experiments, including homonuclear correlation spectroscopy (COSY), heteronuclear multiple bond correlation spectroscopy (HMBC) and heteronuclear single quantum coherence spectroscopy (HSQC), were used to facilitate the assignment of signals. Chemical shift values (δ) are reported in parts per million (ppm), coupling constants (J) are reported in Hertz (Hz), C^q denotes a quaternary carbon, and the spectra are referenced to residual solvent peaks: $CDCl_3$ = 7.26 ppm (^{1}H), 77.16 (^{13}C); DMSO = 2.50 ppm (^{1}H), 39.52 (^{13}C).

Electrospray ionisation mass spectra (ESI) were recorded using a Waters Acquity TQD Tandem Quadrupole mass spectrometer with either acetonitrile or methanol as the carrier solvent. Atmospheric pressure solids analysis probe (ASAP) ionization mass spectra were obtained using a LCT Premier XE mass spectrometer and an Acquity UPLC from Waters Ltd at 350°C. High-resolution mass spectra were obtained using a Quantum time-of-flight (QTof) mass spectrometer.

Theory

To assist the interpretation of the experimental results, we have performed density functional theory (DFT) and time-dependent density functional theory (TD DFT) simulations with the Tamm-Dancoff approximation (TDA) on the monoplatinum(II) complexes using the ORCA 4.2.1 quantum chemistry software[1–3]. All molecular orbital (MO) iso surfaces were visualised using Gabedit 2.5.0.[4]

Geometry optimisations of complexes **1**-**5** in the ground state were performed at the B3LYP[5,6]/def2-SVP[7] level of theory. Triplet excited state (T_1) geometries of dimers of complexes **1**-**5**, and trimers and tetramers of complex **4** were performed at the BP86[8]/def2-SVP[7] level of theory using the RI keyword and def2-SVP/C[9] and def2/J[10] auxiliary basis sets. Single point energy (SPE) calculations were performed at the B3LYP[5,6]/def2-SVP[7] level of theory with the aid of RIJCOSX[11,12] approximation and using CPCM for CH_2Cl_2 in all cases. All calculations were performed using a dense grid (Grid6, GridX6), and *very tight* geometry and SCF convergence criteria and using the atom-pairwise dispersion correction with the Becke-Johnson damping scheme (D3BJ).[13,14] Frequency calculations found all respective optimised geometries to be local minima.

Electrochemistry

Cyclic voltammetry was conducted in a three-electrode, one-compartment cell. All measurements were performed using 0.1 M Bu_4NBF_4 (99%, Sigma Aldrich, dried) solution in dichloromethane (ExtraDry AcroSeal®, Acros Organics). All solutions were purged with nitrogen prior to measurements, which were conducted under a nitrogen atmosphere. The electrodes were: working (Pt disc, d = 1 mm), counter (Pt wire), reference (Ag/AgCl calibrated against ferrocene). All cyclic voltammetry measurements were performed at room temperature with a scan rate of 50 mV s^{-1}.

The ionization potential (IP) and electron affinity (EA) are obtained from onset redox potentials; these figures correspond to HOMO and LUMO values, respectively. The ionization potential is calculated from the onset oxidation potential $IP = E_{ox}^{CV} + 5.1$ [eV] and the electron affinity is calculated from

the onset reduction potential EA = E_{red}^{CV} + 5.1 [eV].[15],[16],[17],[18] An uncertainty of ±0.02 V can be assumed for the electrochemical onset potentials.

Photophysics

Absorption spectra of ~10^{-5} M solutions were recorded with UV-3600 double beam spectrophotometer (Shimadzu). Photoluminescence (PL) spectra of solutions and films were recorded using a QePro compact spectrometer (Ocean Optics) or a Fluorolog fluorescence spectrometer (Jobin Yvon). Time-resolved decays in solution and film were recorded with a Horiba DeltaFlex TCSPC system using a 330 nm SpectraLED light source. Temperature-dependent experiments were conducted using a liquid nitrogen cryostat VNF-100 (sample in flowing vapour, Janis Research) under nitrogen atmosphere, while measurements at room temperature were recorded under vacuum in the same cryostat. Solutions were degassed using five freeze-pump-thaw cycles. Thin films in PVK and pristine layers were deposited from chloroform solutions; pristine films were also thermally evaporated. The photoluminescence quantum yield in film was obtained using an integrating sphere (Labsphere) coupled with a 365 nm LED light source and a QePro (Ocean Optics) detector.

OLED devices

OLEDs were fabricated by vacuum thermal evaporation method. The hole-injection layer (HAT-CN) was deposited first, followed by the hole-transport / electron-blocking layer (TSBPA). Subsequently, **2** or **4** were evaporated as the emissive layer. PO-T2T served as the electron transport/hole blocking layer, while LiF was the electron injection layer and Al the cathode. Devices of 4 × 2 mm pixel size were fabricated. Dipyrazino[2,3-f :2',3'-h]quinoxaline-2,3,6,7,10,11-hexacarbonitrile (HAT-CN, Lumtec, sublimed), 4,4'-(diphenylsilanediyl)bis(*N*,*N*-diphenylaniline) (TSBPA, Lumtec, sublimed), 2,4,6-Tris[3-(diphenylphosphinyl)phenyl]-1,3,5-triazine (PO-T2T, LUMTEC), 1,3-bis(carbazol-9-yl)benzene (mCP, Lumtec, sublimed), 1,3,5-tri[(3-pyridyl)-phen-3-yl]benzene (TmPyPB, Lumtec), LiF (99.995%, Sigma Aldrich), and Aluminium pellets (99.9995%, Lesker) were purchased from the companies indicated in parentheses. We used pre-patterned indium-tin-oxide (ITO)-coated glass substrates with a sheet resistance of 20 Ω cm^{-2} and ITO thickness of 100 nm. The substrates were pre-cleaned with oxygen plasma before use. All organic and inorganic layers were thermally evaporated using Kurt J. Lesker Spectros II deposition system at a base pressure of 10^{-6} mbar. All organic materials and aluminium were deposited at a rate of 1 Å s^{-1} except for the EML which was deposited at a rate of 0.1–0.3 1 Å s^{-1}. The LiF layer was deposited at a rate of 0.1–0.2 Å s^{-1}. Characterisation of OLED devices was conducted in a 10-inch integrating sphere (Labsphere) connected to a Source Measure Unit Keithley 2400 and coupled with a spectrometer USB4000 (Ocean Optics). Further details are available in reference [19].

2. Synthesis

Complexes **1** and **3** were prepared as described elsewhere.[20,21] Complexes **2** and **4** were prepared from the corresponding N^CH^N proligands, which were synthesized by stepwise cross-coupling reactions, as described below.

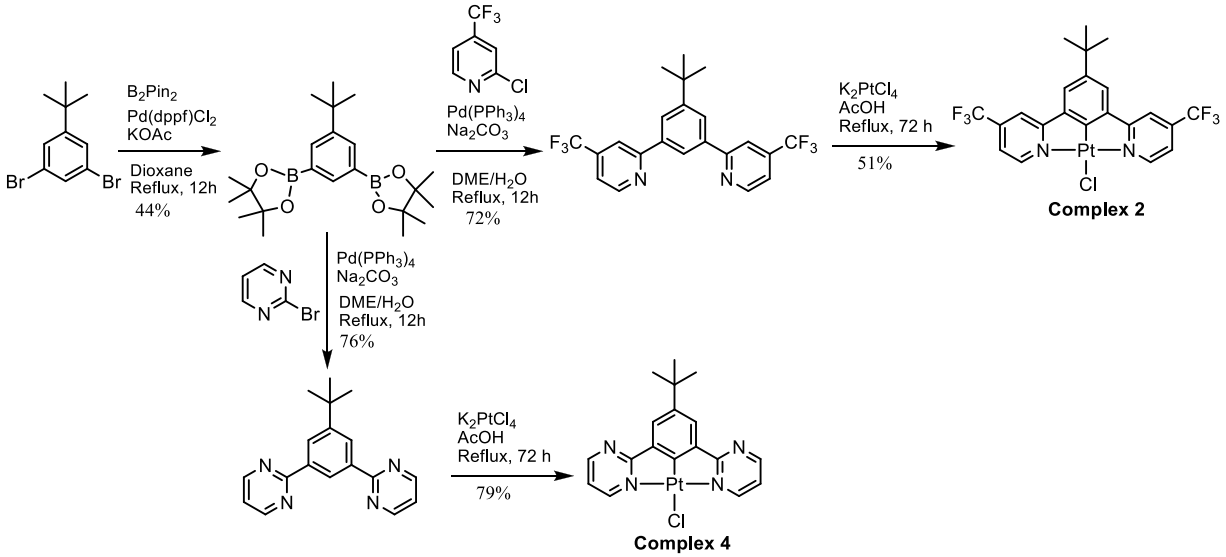

Scheme S1. Synthetic route to complex **2** and **4**.

1-Tert-butyl-3,5-bis(4,4,5,5-tetramethyl-1,3,2-dioxaborolan-2-yl)benzene

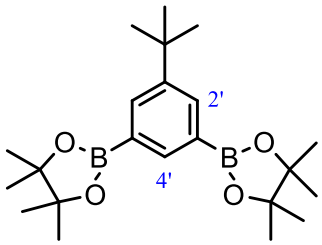

1,3-Dibromo-5-tert-butylbenzene (1.62 g, 5.56 mmol), bis(pinacolato)diboron (3.29 g, 12.9 mmol) and KOAc (3.27 g, 33.3 mmol) were added with 1,4-dioxane (35 mL) to a dry Schlenk flask and degassed by three freeze-pump-thaw cycles. Pd(dppf)Cl_2 (408 mg, 0.558 mmol) was added under a flow of nitrogen and the reaction mixture heated at 80°C overnight under nitrogen. The dioxane solvent was removed under reduced pressure and the crude solid was filtered and washed with CH_2Cl_2 to extract the product. After removal of the solvent under reduced pressure, the crude product was purified by column chromatography on silica (gradient elution, CH_2Cl_2 / MeOH = 100:0 → 98:2) to afford an off-white solid (946 mg, 44%). R_f = 0.4 (silica, CH_2Cl_2). ^{1}H NMR (700 MHz, $CDCl_3$): δ_H = 8.10 (1H, t, ^{4}J 1.2, H^4), 7.91 (2H, d, ^{4}J 1.2, H^2), 1.35 (9H, s, C$(CH_3)_3$), 1.33 (24H, s, OC$(CH_3)_2$). ^{13}C{^{1}H} NMR (176 MHz, $CDCl_3$): δ_C = 149.3 (s, C^1), 138.7 (s, C^4), 134.5 (s, C^2), 83.6 (s, O<u>C</u>$(CH_3)_2$, 34.7 (s, <u>C</u>$(CH_3)_3$), 31.4 (s, C(<u>C</u>$H_3)_3$), 24.86 (s, OC(<u>C</u>$H_3)_2$. MS (AP$^+$): *m/z* = 387.2 [^{11}B, M + H]$^+$, 385.2 [10%, ^{10}B, M + H]$^+$. HRMS (AP$^+$): m/z = 385.2921 [M + H]$^+$, calculated for [$C_{22}H_{37}O_4{}^{10}B_2$] 385.2951.

1,3-Bis(4-(trifluoromethyl)-2-pyridyl)-5-tert-butylbenzene

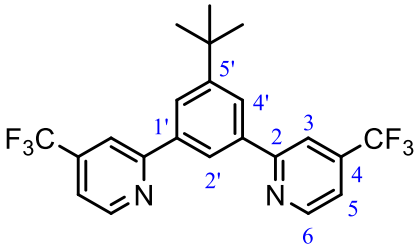

A mixture of 1-tert-butyl-3,5-bis(4,4,5,5-tetramethyl-1,3,2-dioxaborolan-2-yl)benzene (299 mg, 0.774 mmol), 2-chloro-4-(trifluoromethyl)pyridine (270 mg, 1.48 mmol), Na_2CO_3 (1M, in 6.5 mL water), and ethylene glycol dimethyl ether (6.5 mL) was degassed using three freeze-pump-thaw cycles. $Pd(PPh_3)_4$ (44 mg, 0.038 mmol) was added under a flow of nitrogen and the reaction mixture heated at reflux overnight under nitrogen (85°C, 20 h). The crude mixture was washed with water and extracted into dichloromethane (DCM) (3 × 30 mL) before drying over anhydrous $MgSO_4$. The solution was filtered and the solvent was removed under reduced pressure before purification by column chromatography (silica, hexane / EtOAc 100:0 → 80:20). The pure product was obtained as a white solid (236 mg, 72%). R_f = 0.6 (silica, hexane / EtOAc 80:20). ^{1}H NMR (700 MHz, $CDCl_3$): δ_H = 8.91 (2H, d, ^{3}J 5.0, H^6), 8.43 (1H, t, ^{4}J 1.7, $H^{2'}$), 8.17 (2H, d, ^{4}J 1.6, $H^{4'}$), 8.02 - 7.99 (2H, m, H^3), 7.48 (2H, d, ^{3}J 5.0, H^5) 1.47 (9H, s, CH_3). ^{13}C {^{1}H} NMR (176 MHz, $CDCl_3$): δ_C = 158.8 (s, C^2), 152.9 (s, $C^{5'}$), 150.7 (s, C^6), 139.2 (q, J(^{19}F) 33.9, C^4), 138.7 (s, $C^{1'}$), 125.7 (s, $C^{4'}$), 123.2 (s, $C^{2'}$), 122.9 (q, J(^{19}F) 273.0, CF_3), 117.7 (q, J(^{19}F) 3.5, C^5), 116.3 (q, J(^{19}F) 3.6, C^5), 35.2 (s, $\underline{C}(CH_3)_3$), 31.4 (s, $C(\underline{C}H_3)_3$). ^{19}F NMR (376 MHz, $CDCl_3$): δ_F = –64.6. MS (ES^+): m/z = 425.2 $[M + H]^+$. HRMS (ES^+): m/z = 425.1449 $[M + H]^+$, calculated for $[C_{22}H_{19}N_2F_6]$ 425.1452.

1,3-Di(2-pyrimidyl)-5-tert-butylbenzene

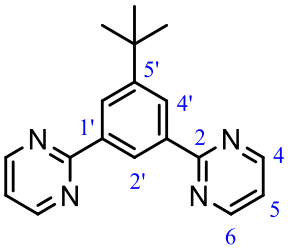

A mixture of 1-tert-butyl-3,5-bis(4,4,5,5-tetramethyl-1,3,2-dioxaborolan-2-yl)benzene (287 mg, 0.743 mmol), 2-bromopyrimidine (225 mg, 1.42 mmol), Na_2CO_3 (1M, in 6 mL water), and ethylene glycol dimethyl ether (6 mL) was degassed using three freeze-pump-thaw cycles. $Pd(PPh_3)_4$ (43 mg, 0.037 mmol) was added under a flow of nitrogen and the reaction mixture heated at reflux overnight under nitrogen (85°C, 20 h). The crude mixture was washed with water and extracted into CH_2Cl_2 (3 × 30 mL) before drying over anhydrous $MgSO_4$. The solution was filtered and the solvent removed under reduced pressure before purification by column chromatography (silica, hexane/EtOAc 100:0 → 30:70). The product was obtained as a white solid (236 mg, 76%). R_f = 0.2 (silica, hexane/EtOAc 70:30). ^{1}H NMR (700 MHz, $CDCl_3$): δ_H = 9.36 (1H, t, ^{4}J 1.6, $H^{2'}$), 8.84 (4H, d, ^{3}J 4.8, H^4), 8.64 (2H, d, ^{4}J 1.6, $H^{4'}$), 7.19 (2H, t, ^{3}J 4.8, H^5). ^{13}C {^{1}H} NMR (176 MHz, $CDCl_3$): δ_C = 164.9 (s, C^2), 157.2 (s, C^4), 152.1 (s, $C^{5'}$), 137.8 (s, $C^{1'}$), 127.5 (s, $C^{4'}$), 125.7 (s, $C^{2'}$), 119.1 (s, C^5), 35.1 (s, $\underline{C}(CH)_3$), 31.5 (s, $C(\underline{C}H_3)_3$). MS (ES^+): m/z = 291.3 $[M + H]^+$. HRMS (ES^+): m/z = 291.1612 $[M + H]^+$, calculated for $[C_{18}H_{19}N_4]$ 262.1610.

Complex 2

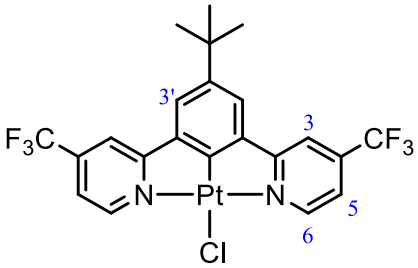

A mixture of the proligand 1,3-bis(4-trifluoromethyl-pyrid-2-yl)-5-*tert*-butylbenzene (109 mg, 0.257 mmol) and K_2PtCl_4 (118 mg, 0.284 mmol) in acetic acid (13 mL) was heated under a nitrogen atmosphere for 72 h after degassing by three freeze-pump-thaw cycles. The precipitated material was washed sequentially with water, ethanol, and diethyl ether, giving the desired product as an orange solid (86 mg, 51%). ^{1}H NMR (700 MHz, $CDCl_3$, δ_H): 9.47 (2H, d, *J* = 5.9, $^3J(^{195}Pt)$ = 42, H^6), 7.86 (2H, d, *J* = 1.8, H^3), 7.62 (2H, s, $H^{3'}$), 7.45 (2H, dd, *J* = 5.9, 1.8, H^5), 1.45 (9H, s, CH_3). ^{19}F NMR (376 MHz, $CDCl_3$, δ_F): –65.0. ESMS$^+$: *m/z* = 658.9 [^{195}Pt, M + CH_3CN – Cl]$^+$, 658.2 [66%, ^{194}Pt, M + CH_3CN – Cl]$^+$. HRMS (ESI$^+$): *m/z* = 658.1208 [M + CH_3CN – Cl]$^+$, calcd for [$C_{24}H_{20}N_3F_6{}^{194}Pt$] 658.1188. Anal. calcd for $C_{22}H_{17}ClF_6N_2Pt$: 40.41; H, 2.62; N 4.28 %; found C, 40.02; H, 2.59; N 4.26 %.

Complex 4

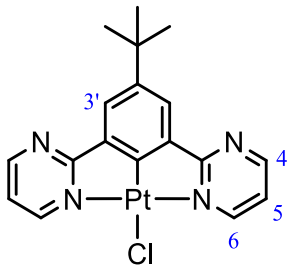

A mixture of the proligand 1,3-di(2-pyrimidyl)-5-tert-butylbenzene (103 mg, 0.355 mmol) and K_2PtCl_4 (169 mg, 0.407 mmol) in glacial acetic acid (14 mL) was heated under a nitrogen atmosphere for 72 h after degassing by three freeze-pump-thaw cycles. The precipitated material was washed sequentially with water, ethanol, and diethyl ether, giving the desired product as a green-yellow solid (146 mg, 79%). ^{1}H NMR (700 MHz, $(CD_3)_2SO$): δ_H = 9.19 (2H, dd, ^{3}J 5.7, ^{4}J 2.2, $^3J(^{195}Pt)$ = 40*, H^6), 9.10 (2H, dd, ^{3}J 4.8, 2.2, H^4), 7.80 (2H, s, $H^{3'}$), 7.60 (2H, dd, ^{3}J 5.7, 4.8, H^5). MS (AP$^+$): m/z = 525.1 [^{195}Pt, M + CN - Cl]$^+$, 524.2 [57%, ^{194}Pt, M + CH_3CN - Cl]$^+$. HRMS (AP$^+$): m/z = 524.1351 [M + CH_3CN - Cl]$^+$, calculated for [$C_{20}H_{20}N_5{}^{194}Pt$]$^+$ 524.1345. Anal. $C_{18}H_{17}ClN_4Pt$ (519.90): calculated C, 41.58; H, 3.30; N 10.78; found C, 41.24; H, 3.32; N 10.60.

* At the frequency of 700 MHz employed, the satellites for coupling of H^6 to ^{195}Pt are not well resolved, owing to the effects of chemical shift anisotropy,[22] the indicated value is thus an estimate.

3. Crystallography

The X-ray single crystal data have been collected using λMoKα radiation (λ =0.71073Å) on a Bruker D8Venture 3-circle diffractometer (Photon100 CMOS detector, IμS-microsource for **2-CHCl$_3$**, **3** and **4**; Photon III MM C14 CPAD detector, IμS-III-microsource, focusing mirrors for **2-MeOH**) equipped with a Cryostream (Oxford Cryosystems) open-flow nitrogen cryostat at the temperature of 120.0(2)K. All structures were solved by direct methods and refined by full-matrix least squares on F^2 for all data using Olex2[23] and SHELXTL[24] software. All non-hydrogen atoms were refined in anisotropic approximation; hydrogen atoms were placed in the calculated positions and refined in riding mode. Disordered atoms in structure **2-MeOH** were refined with fixed SOF = 0.5 (CF_3 groups) and 0.25 (MeOH solvent molecules). Crystallographic data for the structures have been deposited with the Cambridge Crystallographic Data Centre as supplementary publication CCDC 2063390 (**2-CHCl$_3$**) and CCDC 2164616–2164618 (**2-MeOH**, **3**, and **4**). A table of unit cell parameters and other crystal data for the four structures follows on the next page.

Table S3.1. Crystal data and structure refinement parameters.

Compound	**2**-$CHCl_3$	**2**-MeOH	**3**	**4**
Empirical formula	$C_{22}H_{17}ClF_6N_2Pt$ x $CHCl_3$	$C_{22.88}H_{20.88}ClF_6N_2O_{0.88}Pt$	$C_{24}H_{16}ClN_2Pt$	$C_{18}H_{17}ClN_4Pt$
Formula weight	773.28	682.33	562.93	519.90
Temperature/K	120.0	120.0	230	120.0
Crystal system	triclinic	monoclinic	monoclinic	monoclinic
Space group	P-1	$P2_1/c$	C2/c	$P2_1/c$
a/Å	9.6801(7)	14.9746(5)	15.453(2)	6.8240(9)
b/Å	10.9554(8)	23.6254(8)	15.333(2)	21.121(3)
c/Å	12.8666(10)	14.2787(5)	7.9555(13)	11.2367(14)
α/°	68.534(3)	90	90	90
β/°	84.144(3)	113.5820(10)	105.168(5)	90.107(4)
γ/°	78.223(3)	90	90	90
Volume/$Å^3$	1242.56(16)	4629.7(3)	1819.3(5)	1619.5(4)
Z	2	8	4	4
$\rho_{calc}g/cm^3$	2.067	1.958	2.055	2.132
μ/mm^{-1}	6.138	6.243	7.872	8.836
F(000)	740.0	2625.0	1076.0	992.0
Crystal size/mm^3	0.06 × 0.04 × 0.005	0.24 × 0.02 × 0.02	0.239 × 0.13 × 0.053	0.29 × 0.01 × 0.01
Reflections collected	27731	111237	15605	20830
Independent reflections, R_{int}	7266, 0.0524	13487, 0.0693	2669, 0.0349	3545, 0.1113,
Data/restraints/parameters	7266/0/328	13487/122/680	2669/0/129	3545/7/222
Goodness-of-fit on F^2	1.007	1.152	1.038	1.070
Final R_1 indexes [I>=2σ (I)]	0.0298	0.0398	0.0229	0.0494
Final wR_2 indexes [all data]	0.0492	0.0917	0.0489	0.1016

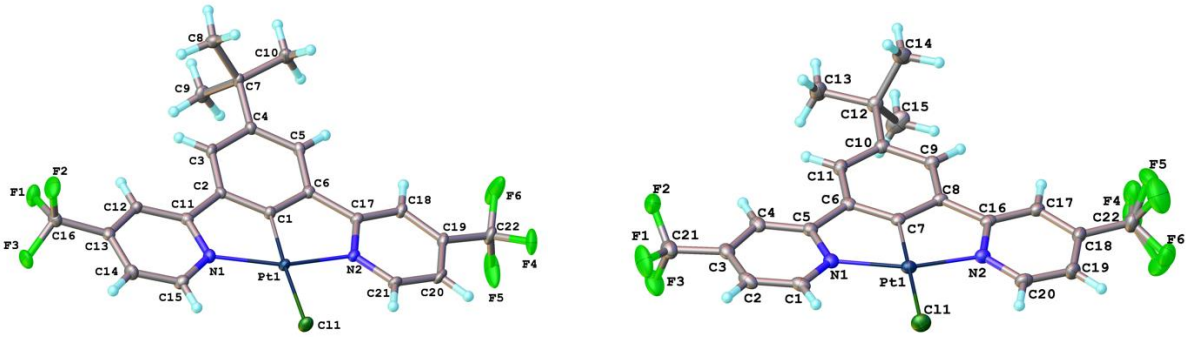

Figure S3.1 Molecular structures of complex **2** as chloroform and methanol solvates (denoted **2**-$CHCl_3$ and **2**-MeOH respectively) in the crystals.

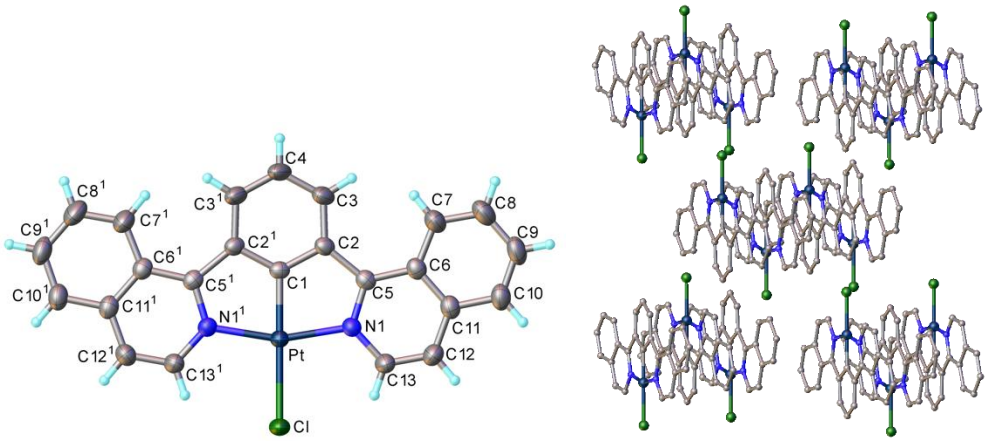

Figure S3.2 Molecular structure of complex **3** and a view of the packing of the molecules in the crystal.

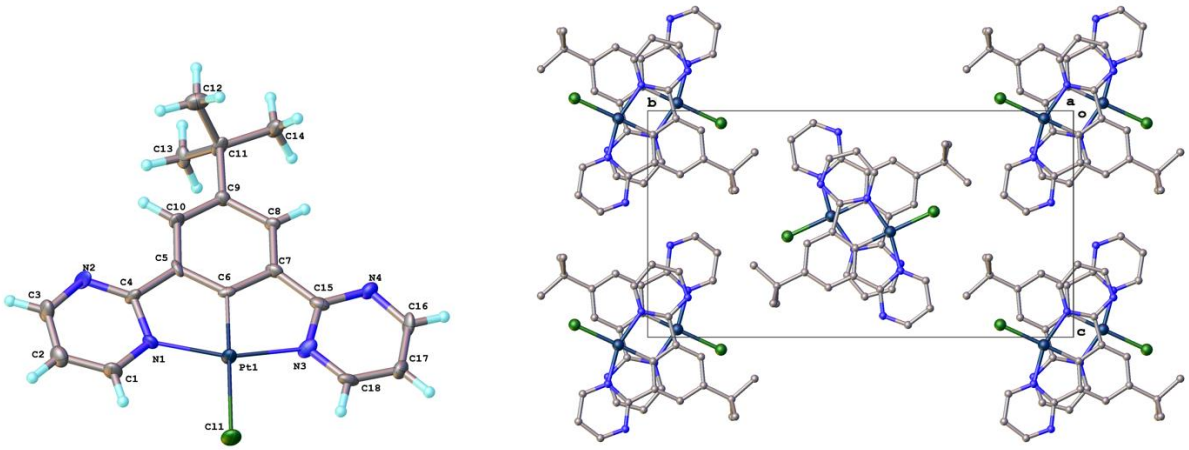

Figure S3.3 Molecular structure of complex **4** and a view of the packing of the molecules in the crystal.

4. Theory

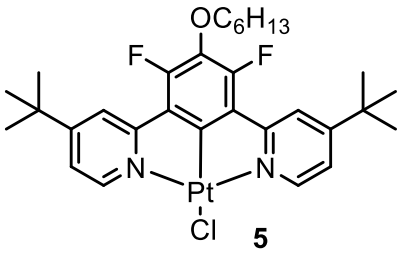

Figure S4.1. Structure of complex **5** reported earlier.[25]

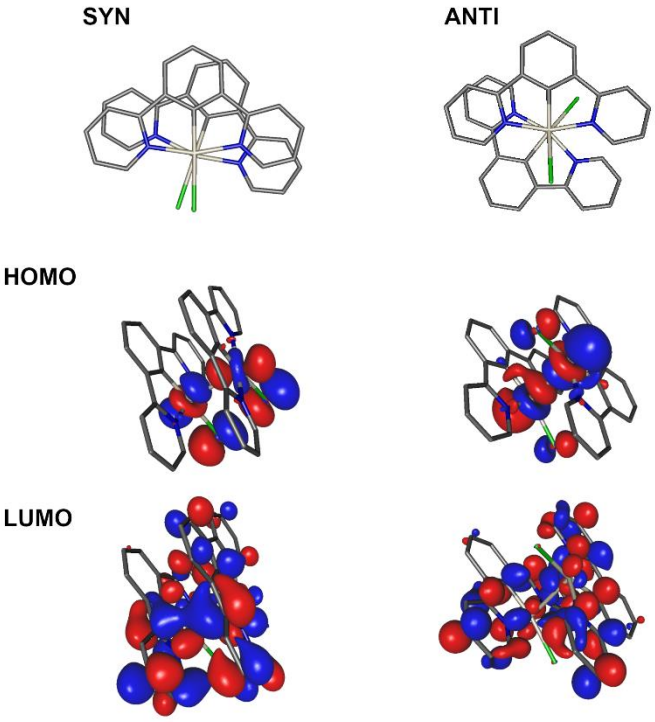

Figure S4.2. Structural geometry and frontier molecular orbital contour plots for *syn* and *anti* excimers/dimers of complex **1**. T_1 geometry of the excimer obtained at BP86/def2-SVP level with subsequent single point energy calculation using B3LYP/def2-SVP/CPCM(CH_2Cl_2) level of theory.

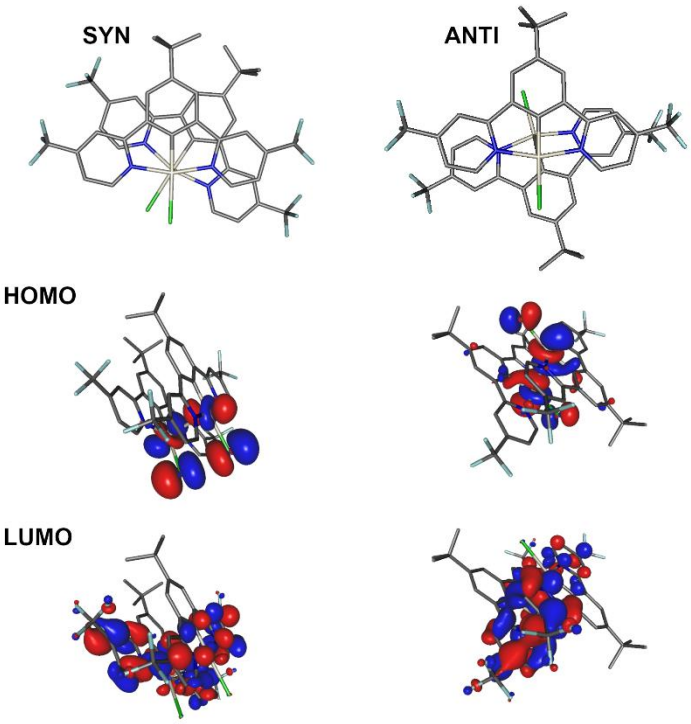

Figure S4.3. Structural geometry and frontier molecular orbital contour plots for *syn* and *anti* excimers/dimers of complex **2**. T_1 geometry of the excimer obtained at BP86/def2-SVP level with subsequent single point energy calculation using B3LYP/def2-SVP/CPCM(CH_2Cl_2) level of theory.

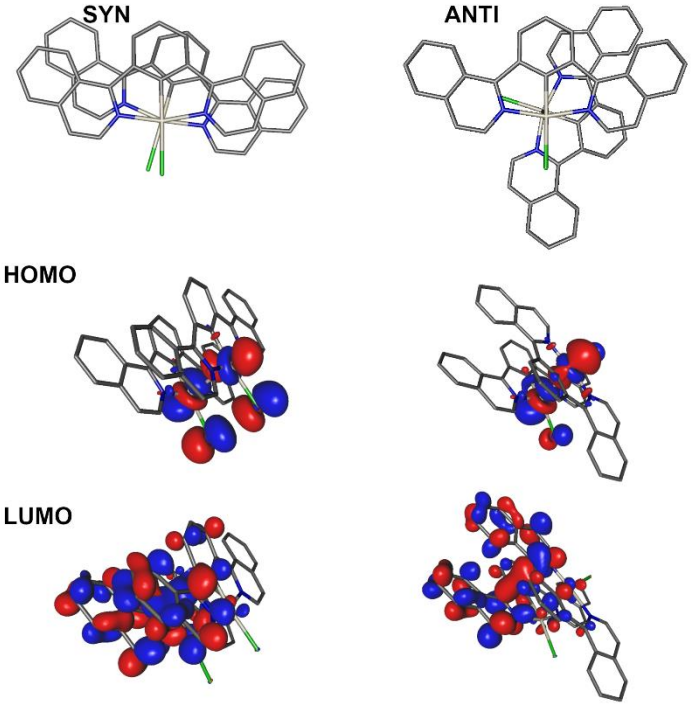

Figure S4.4. Structural geometry and frontier molecular orbital contour plots for *syn* and *anti* excimers/dimers of complex **3**. T_1 geometry of the excimer obtained at BP86/def2-SVP level with subsequent single point energy calculation using B3LYP/def2-SVP/CPCM(CH_2Cl_2) level of theory.

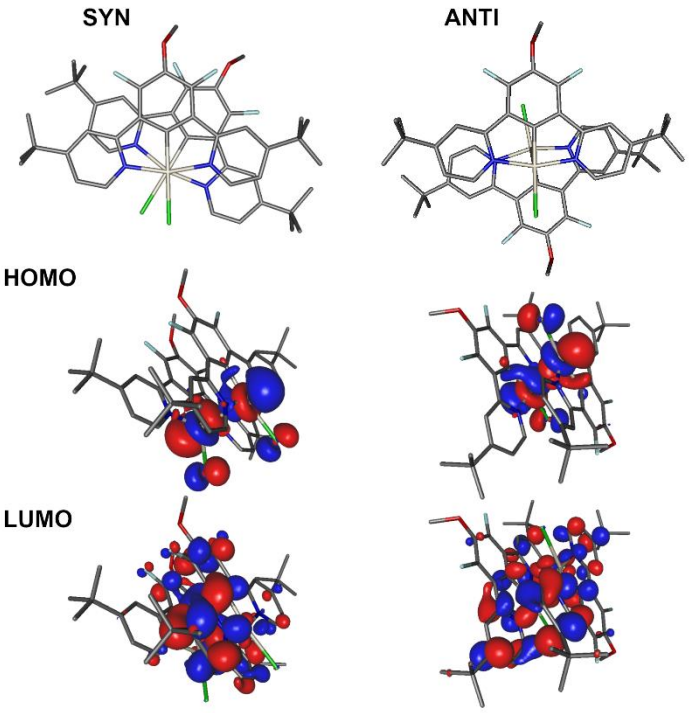

Figure S4.5. Structural geometry and frontier molecular orbital contour plots for *syn* and *anti* excimers/dimers of complex **5**. T_1 geometry of the excimer obtained at BP86/def2-SVP level with subsequent single point energy calculation using B3LYP/def2-SVP/CPCM(CH_2Cl_2) level of theory.

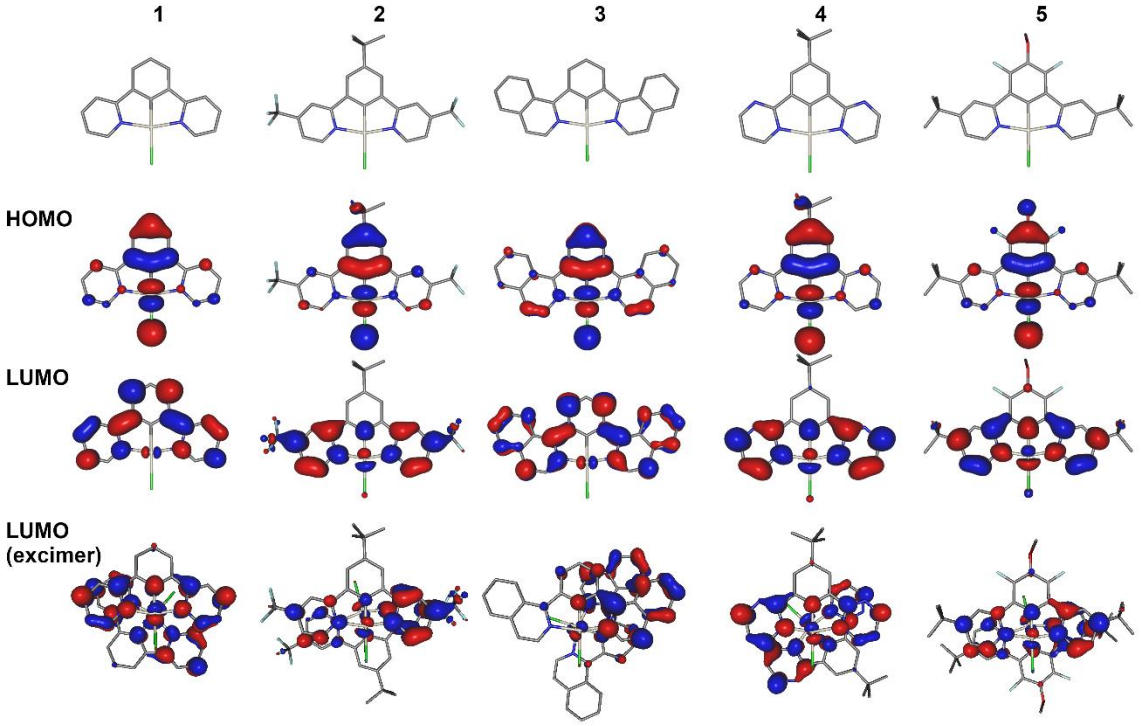

Figure S4.6. Structural geometry (*top*) and frontier molecular orbital contour plots (*middle*) for complexes **1**-**5** at the S_0 geometry obtained at B3LYP/def2-SVP/CPCM(CH_2Cl_2) level of theory. LUMO at the T_1 geometry (BP86/def2-SVP) of the excimer (*bottom*) obtained at B3LYP/def2-SVP/CPCM(CH_2Cl_2) level of theory.

Table S4.1. Calculated properties of dimers/excimers of complexes **1-5** at T_1 geometry using the BP86/def2-SVP level of theory for geometry optimisation. Single point energy obtained at B3LYP/def2-SVP/CPCM(CH_2Cl_2).

Complex	Dimer type	Pt-Pt distance, Å	Cl-Pt-Pt-Cl dihedral, °	$f(S_1 \rightarrow S_0)$	S_1, eV	T_1, eV
1	*syn*	2.90	17.6	0.0145	1.55	1.31
	anti	2.85	137.9	0.0426	1.70	1.39
2	*syn*	2.88	30.4	0.0136	1.45	1.21
	anti	2.95	163.9	0.0149	1.34	1.10
3	*syn*	2.88	16.0	0.0108	1.17	0.93
	anti	2.84	105.6	0.0156	1.21	0.95
4	*syn*	2.80	54.2	0.0302	1.61	1.34
	anti	2.84	131.7	0.0345	1.61	1.31
5	*syn*	2.81	32.7	0.0219	1.76	1.54
	anti	2.90	169.2	0.0301	1.80	1.53

5. Photophysics

a) Solution state

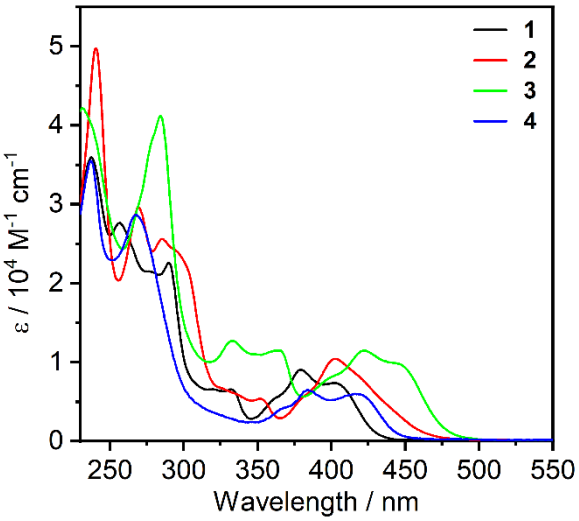

Figure S5.1. Absorption spectra of complexes **1-4** in CH_2Cl_2.

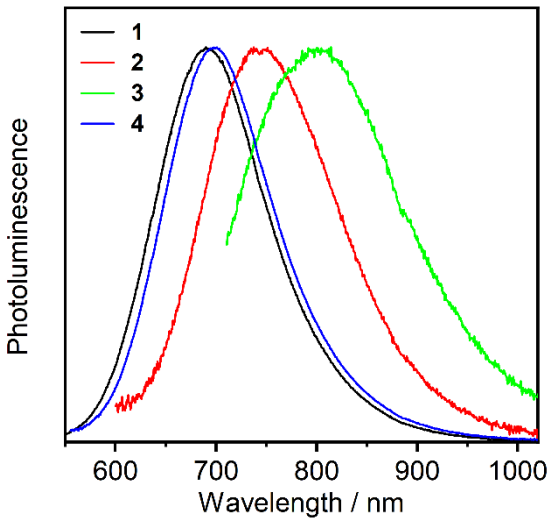

Figure S5.2. Steady state photoluminescence spectra of excimers formed from complexes **1-4** in CH_2Cl_2. Spectra are obtained by subtracting contribution of monomolecular phosphorescence ($c = 10^{-5}$ M) from photoluminescence spectra obtained at high concentrations ($c = 3\times10^{-4}$ M).

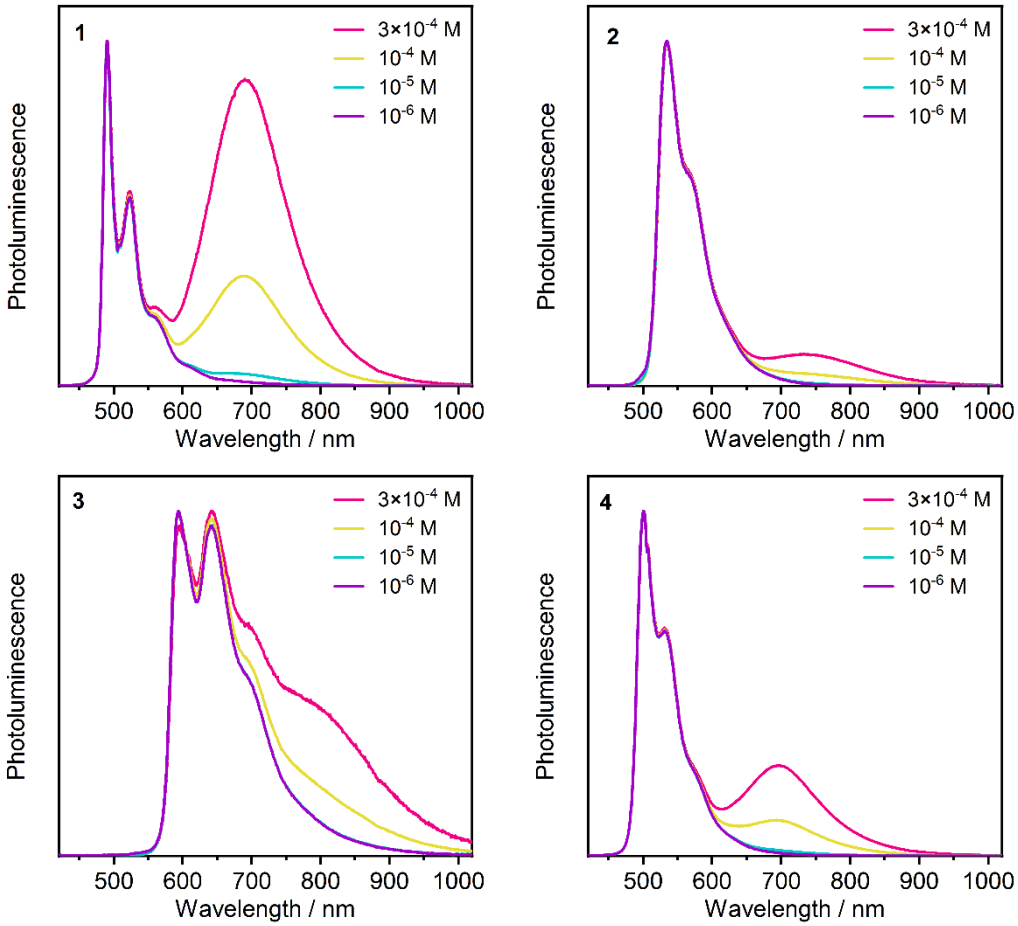

Figure S5.3. Photoluminescence spectra of complexes **1-4** at various concentrations in CH_2Cl_2 indicated in figure legends.

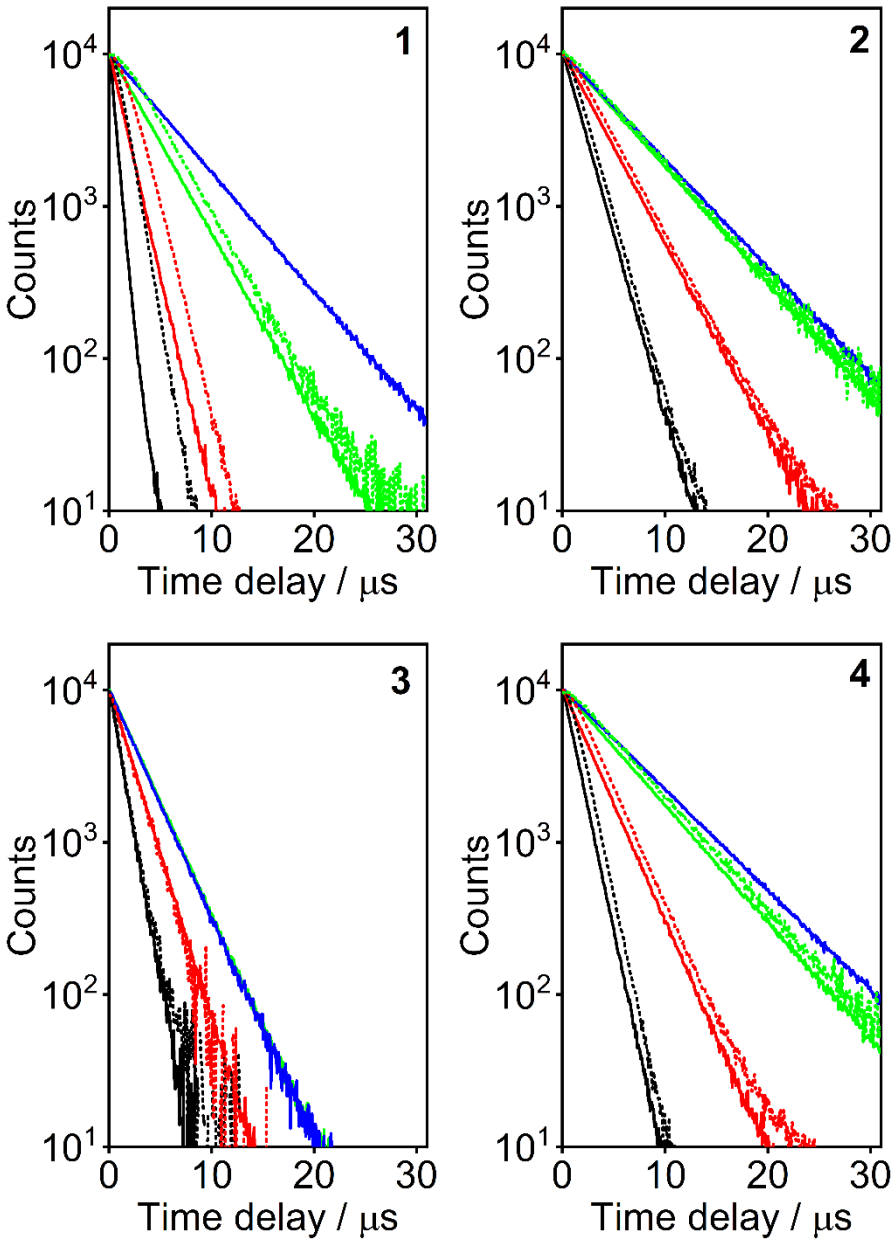

Figure S5.4. Photoluminescence decay traces of monomer (continuous line) and excimer (dotted line) bands of complexes **1-4** at various concentrations in CH_2Cl_2 identified by colour: 3×10^{-4} M – black; 10^{-4} M – red; 10^{-5} M – green; 10^{-6} M – blue.

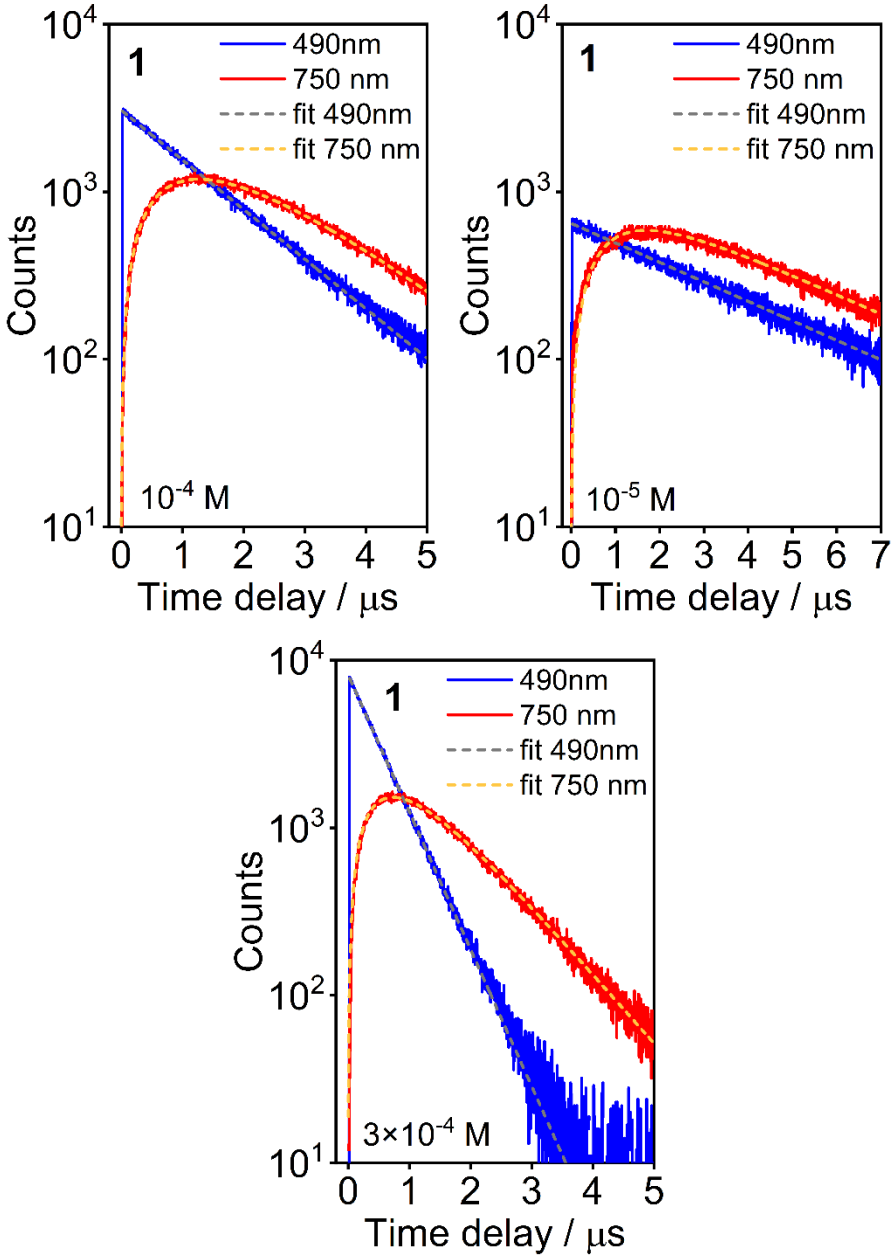

Figure S5.5. Photoluminescence decay traces of monomer (blue line) and excimer (red line) bands of complex **1** at various concentrations in CH_2Cl_2 identified in bottom left corner of each figure. Fitting curves obtained with equations 2 and 4 from the main text are shown as dashed lines.

The biexponential decay of the excimer emission observed in compound **1** at c = 3×10^{-4} M behaves differently from that at lower concentrations (**Figure S5.5**). In this case, the excimer emission rises with a rate equal to the monomer decay rate, and then decays with the excimer decay rate. At this higher concentration, the excimer is formed at a rate faster than that at which it normally decays.

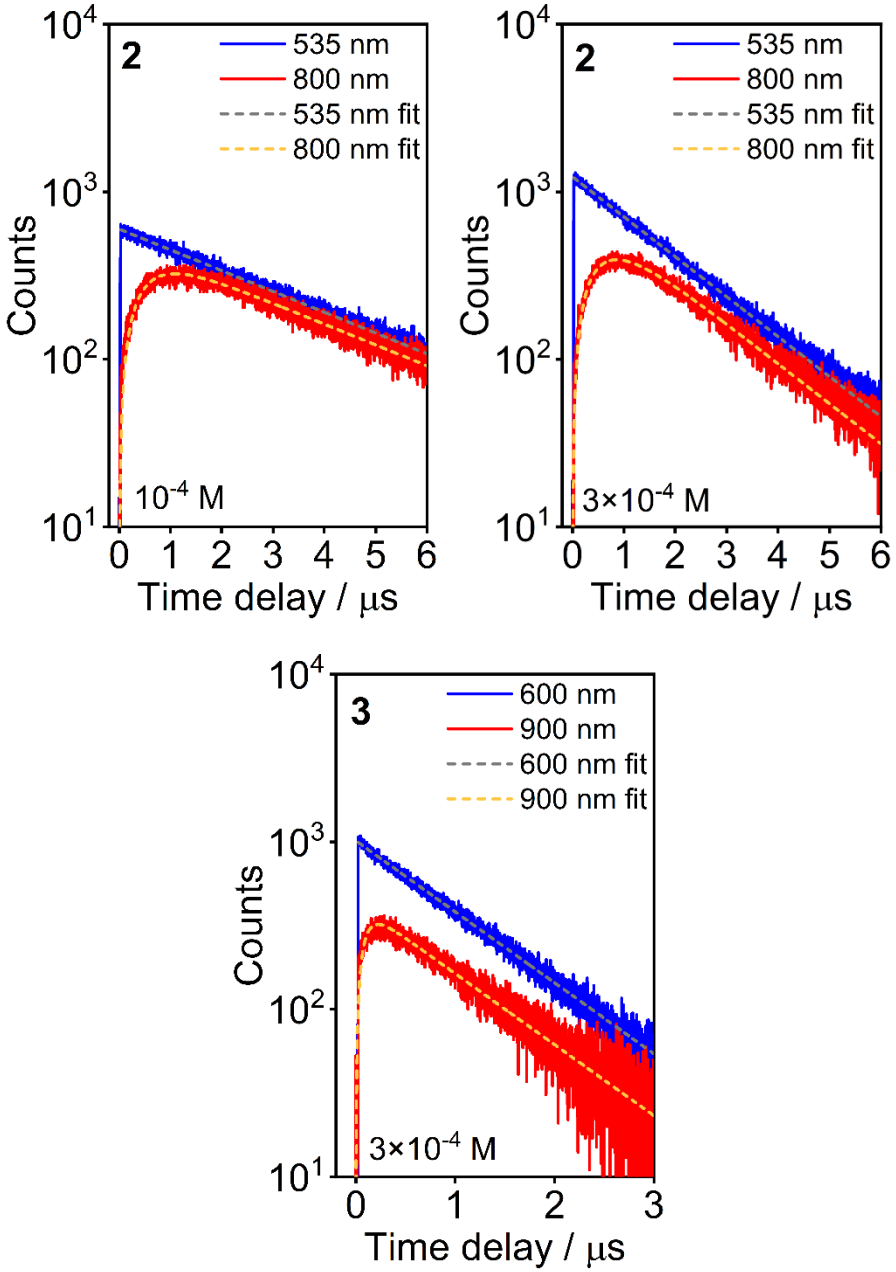

Figure S5.6. Photoluminescence decay traces of monomer (blue line) and excimer (red line) bands of complexes **2** and **3** at various concentrations in CH_2Cl_2 identified in bottom left corner of each figure. Fitting curves obtained with equations 2 and 4 from the main text are shown as dashed lines.

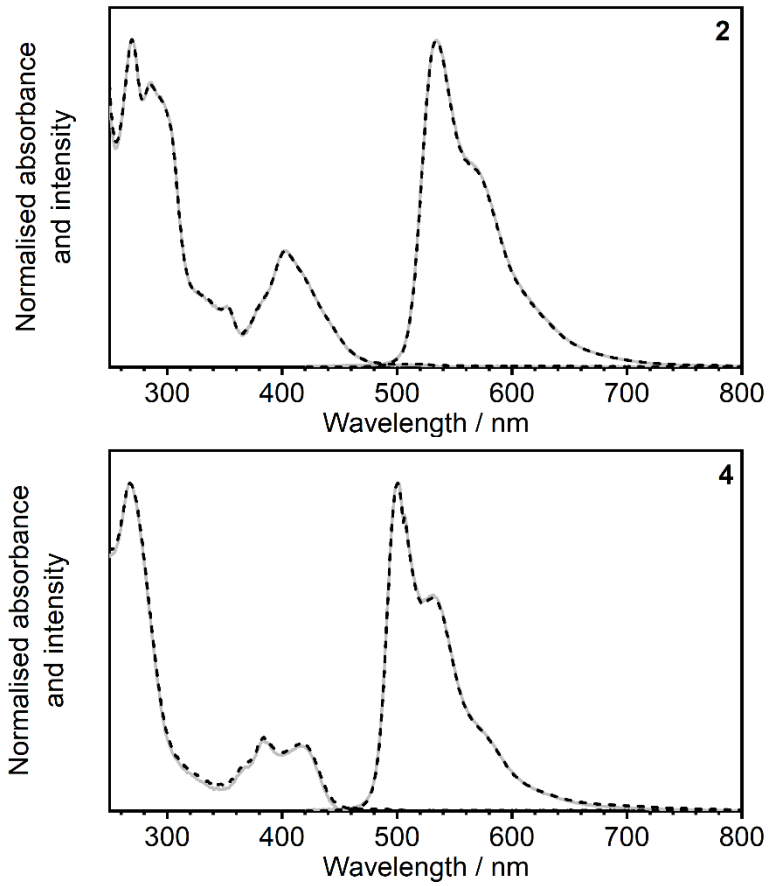

Figure S5.7. Absorption and photoluminescence spectra of complexes **2** and **4** in CH_2Cl_2. Gray continuous line represents original compound, while black dashed line is obtained from a vacuum deposited film.

Table S5.1. Photophysical data for complexes **1**-**4** in deoxygenated CH_2Cl_2 solution at 295 K.

	λ_{abs} / nm (ε / M^{-1} cm^{-1})	λ_{max} / nm (monomer)	λ_{max} / nm (excimer)	Φ_{PL} [(a)]	τ_0 / µs (at c→0)	k_r / 10^5 s^{-1}	k_{nr} / 10^5 s^{-1}
1	485 (200), 403 (7400), 380 (9100), 361sh (5300), 332 (6600), 320 (6600), 290 (22600), 277sh (21500), 257 (27600), 237 (35900)	490, 522, 566sh	690	0.60 [26]	5.7	1.1	0.7
2	516 (200), 403 (10400), 380 (5500), 352 (5376), 289 (25600), 270 (29600), 242 (49800)	534, 573sh	744	0.91	6.3	1.4	0.1
3	584 (100), 540 (100), 446 (9800), 423 (11500), 397 (7800), 363 (11500), 333 (12700), 285 (41200)	593, 642, 699sh	801	0.13	3.1	0.4	2.8
4	485 (300), 416 (6000), 384 (6500), 268 (28700), 237 (35500)	500, 531, 584sh	701	0.49	6.8	0.7	0.8

[(a)] Luminescence quantum yield in deoxygenated solution, measured using $[Ru(bpy)_3]Cl_2$ (aq) as the standard (Φ_{PL} = 0.04).[27]

Table S5.2. Decay and rise time constants and quenching constants for monometallic Pt(II) complexes in CH_2Cl_2 solutions.

Complex	τ_0 / µs (at c→0)	k_Q / 10^9 M^{-1} s^{-1}	c = 1×10^{-5} M			c = 1×10^{-4} M			c = 3×10^{-4} M		
			τ_M / µs	τ_1 / µs	τ_2 / µs	τ_M / µs	τ_1 / µs	τ_2 / µs	τ_M / µs	τ_1 / µs	τ_2 / µs
1	5.7 ±1.1	5.6 ±0.2	3.73	3.73	0.90	1.47	1.47	1.10	0.53*	1.05	0.53
2	6.27 ±0.04	1.3 ±0.1	5.81	-	-	3.50	3.50	0.46	1.82	1.82	0.47
3	3.08 ±0.11	1.95 ±0.08	2.93	-	-	2.00	-	-	1.03	1.03	0.080
4	6.8 ±0.5	1.96 ±0.07	5.69	-	-	3.11	3.11	0.59	1.35	1.35	0.56

* **1** decays biexponentially at c = 3×10^{-4} M: 0.53 ±0.01 (96%); 1.2 ±0.2 (4%) (Eq. 4)

b) Solid film

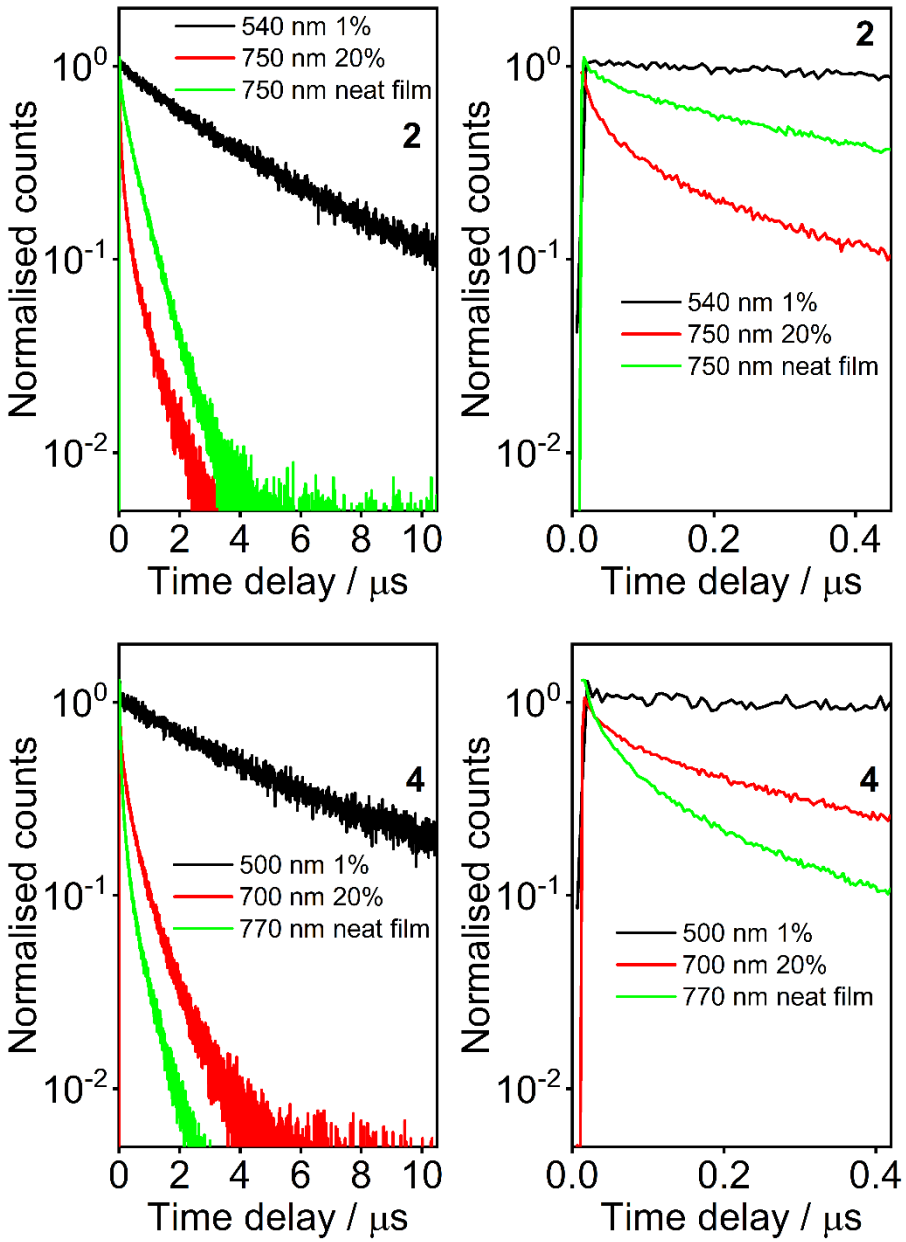

Figure S5.8. Photoluminescence decay of complexes **2** and **4** in solution-processed neat films or films in PVK host.

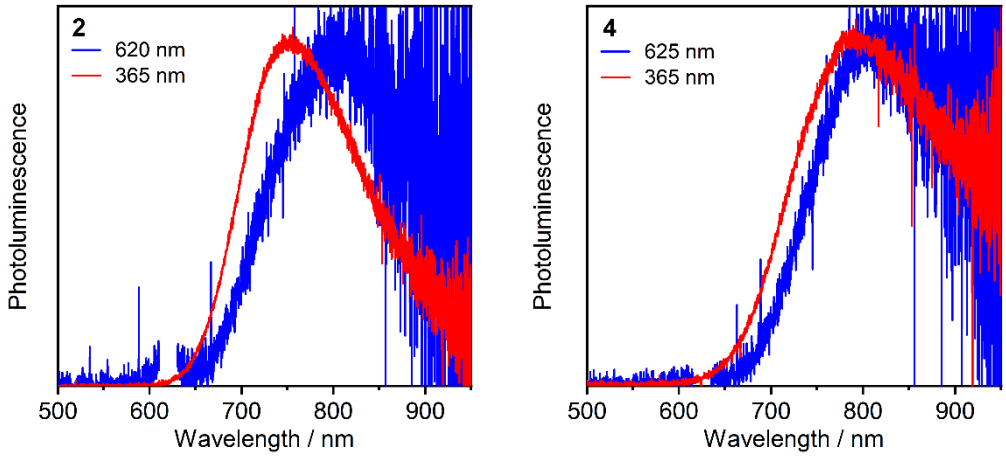

Figure S5.9. Normalised photoluminescence spectra of complexes **2** and **4** in evaporated neat films obtained using a short and long wavelength excitation.

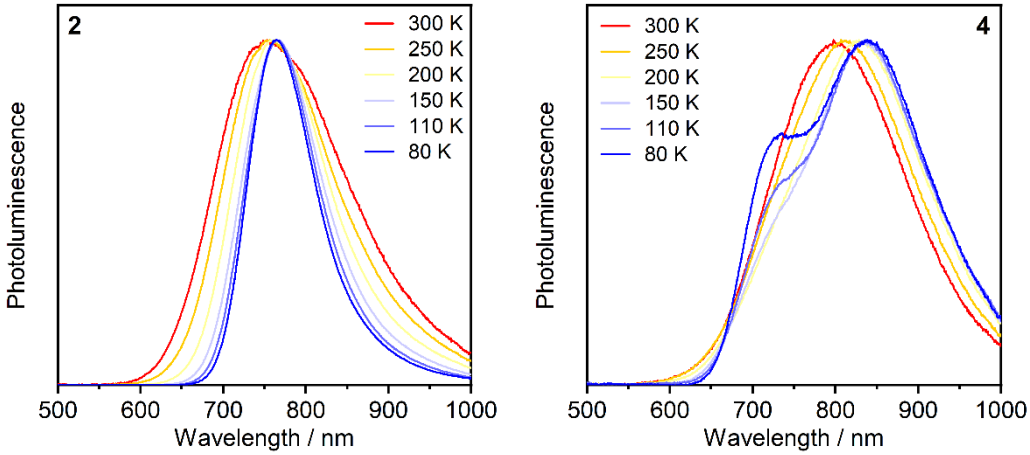

Figure S5.10. Normalised photoluminescence spectra of complexes **2** and **4** in evaporated neat films at various temperatures indicated in figure legends.

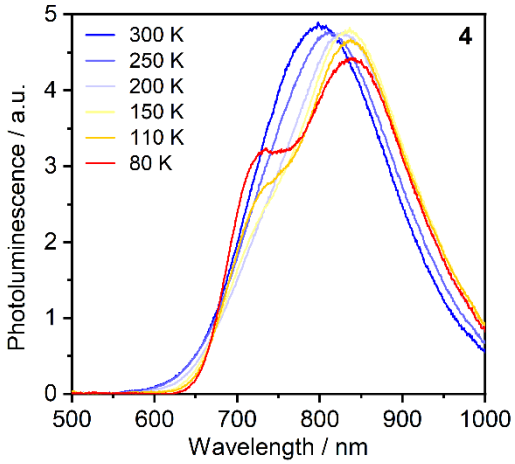

Figure S5.11. Area normalised photoluminescence spectra of complex **4** in evaporated neat film at various temperatures indicated in figure legend.

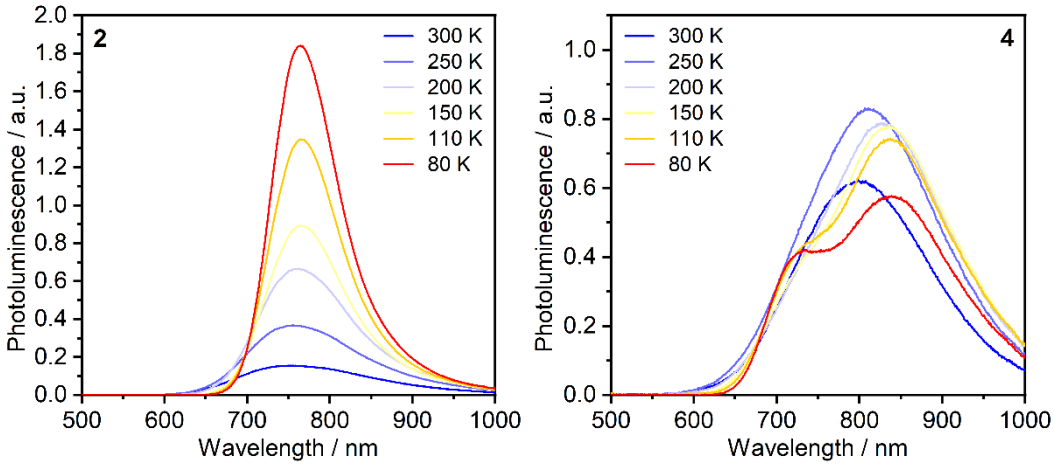

Figure S5.12. Photoluminescence spectra of complexes **2** and **4** in evaporated neat films at various temperatures indicated in figure legends.

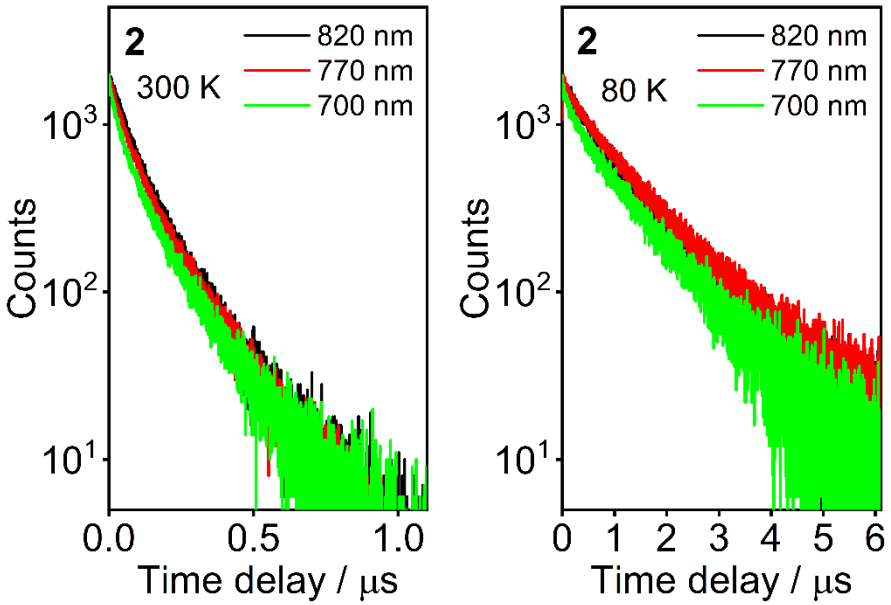

Figure S5.13. Photoluminescence decay traces for complex **2** in neat, evaporated film at 300 and 80 K at wavelengths indicated in figure legends.

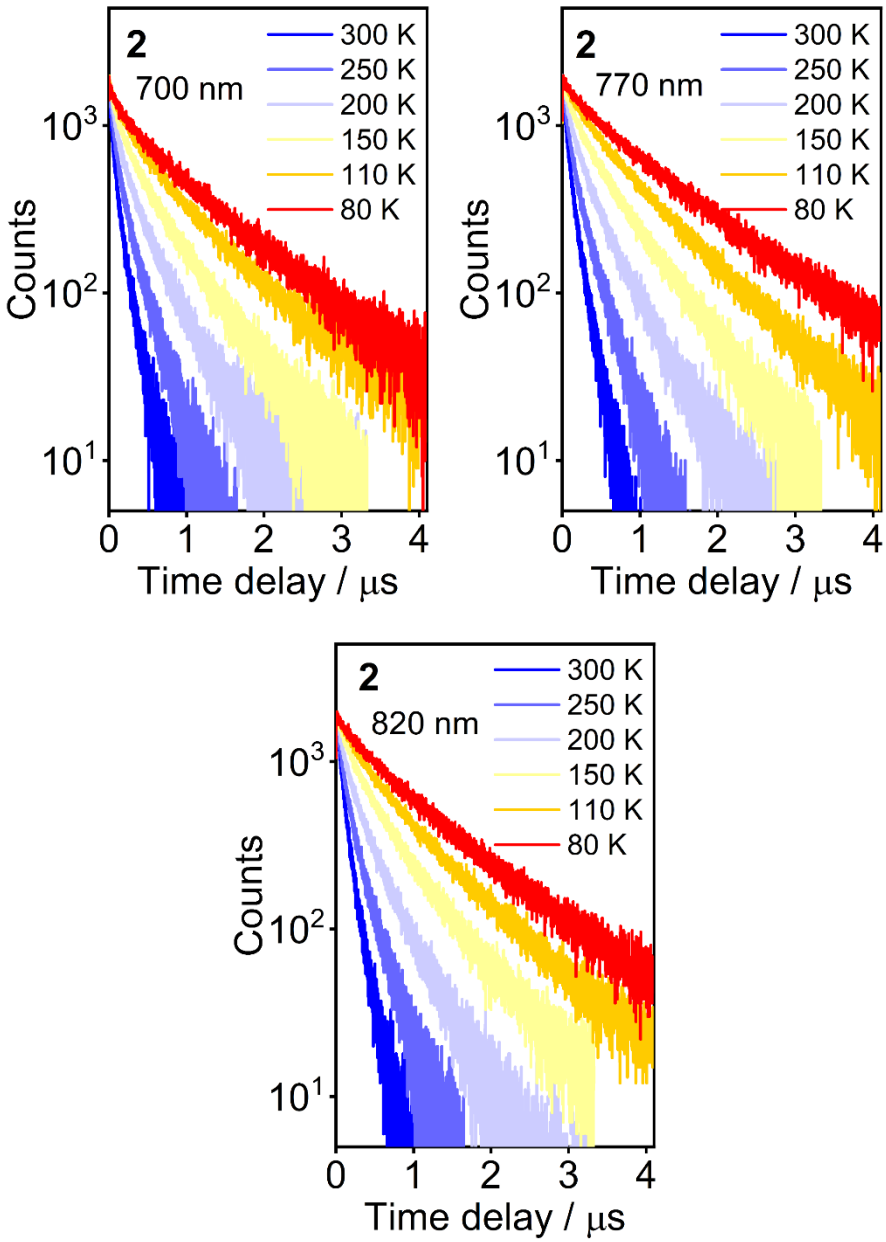

Figure S5.14. Photoluminescence decay traces for complex **2** in neat, evaporated film at temperatures from 300 to 80 K and wavelengths indicated in figure legends.

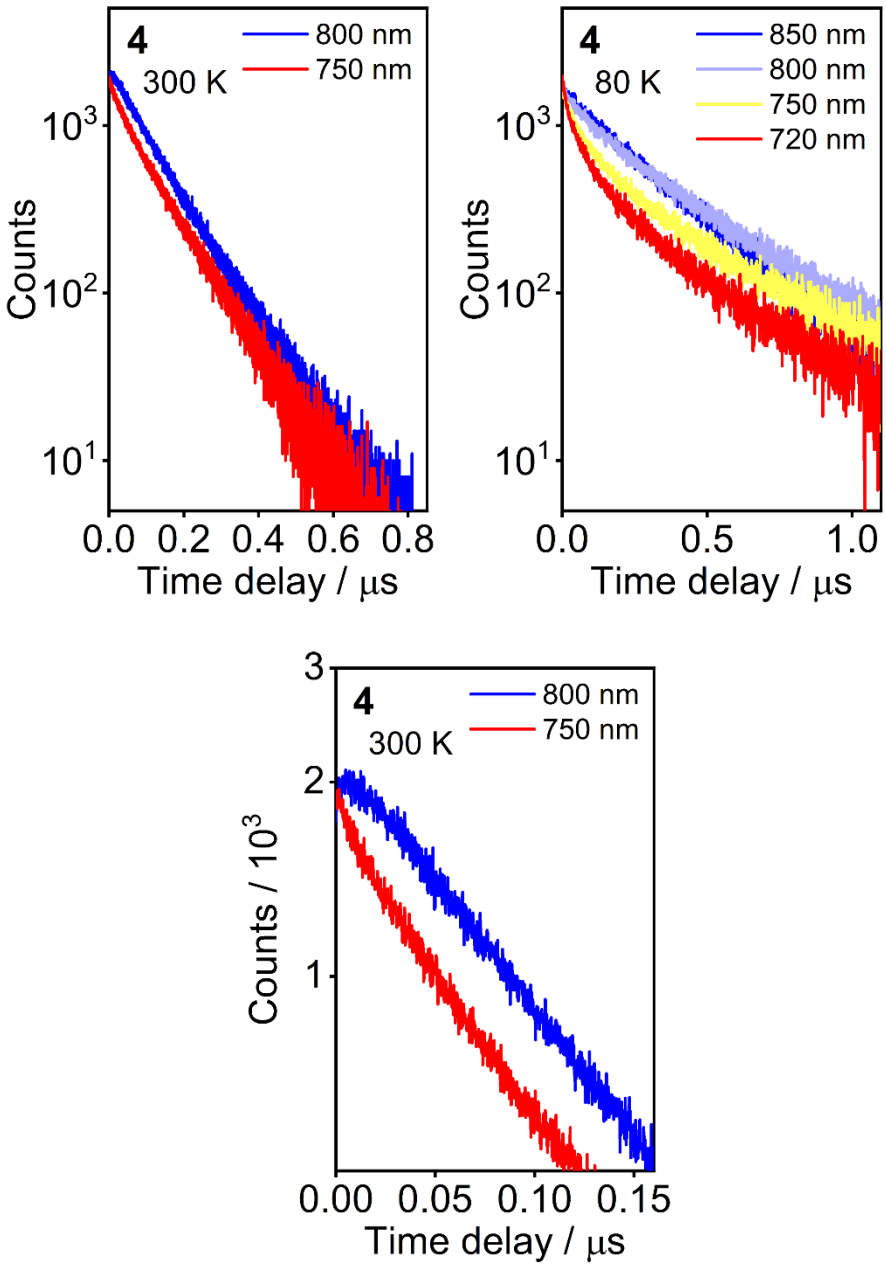

Figure S5.15. Photoluminescence decay traces for complex **4** in neat, evaporated film at 300 and 80 K at wavelengths indicated in figure legends.

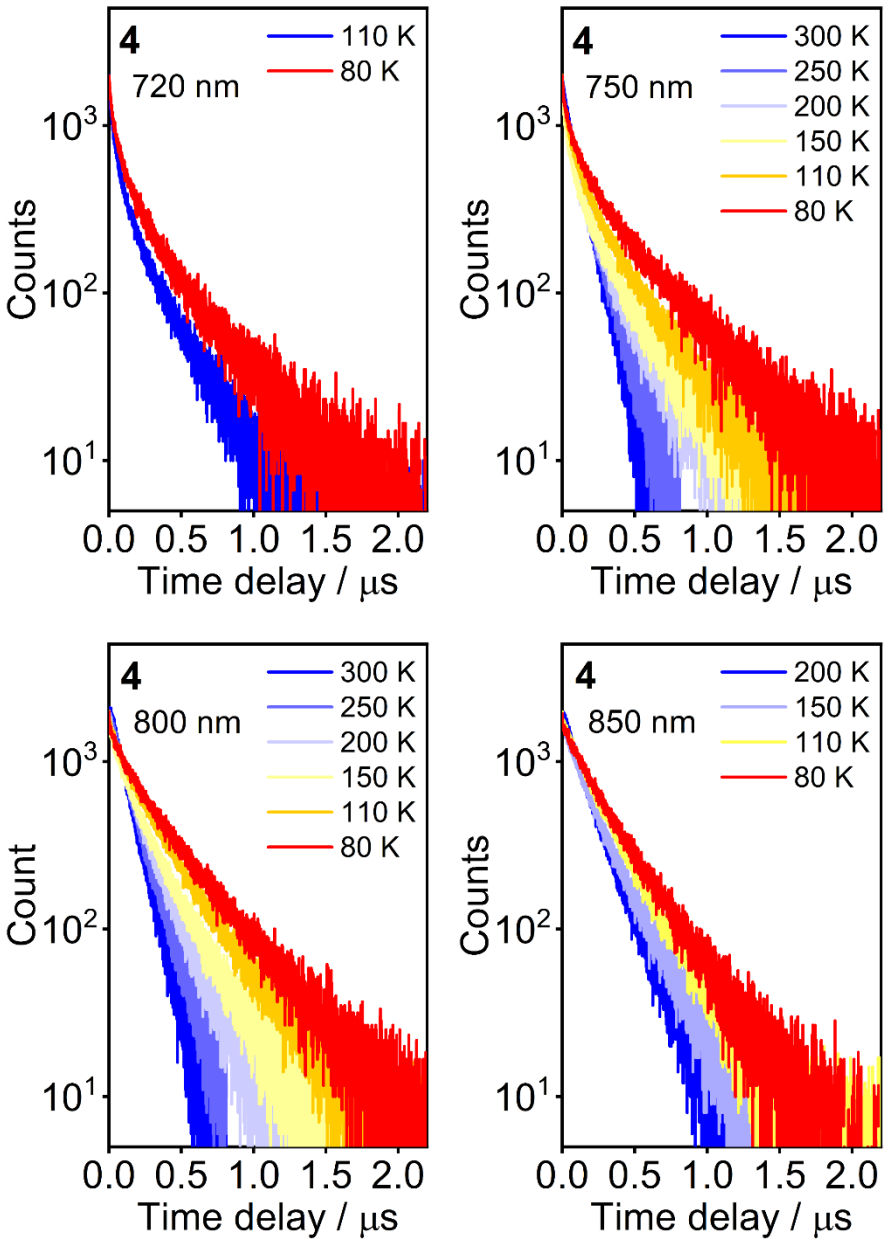

Figure S5.16. Photoluminescence decay traces for complex **4** in neat, evaporated film at temperatures from 300 to 80 K and wavelengths indicated in figure legends.

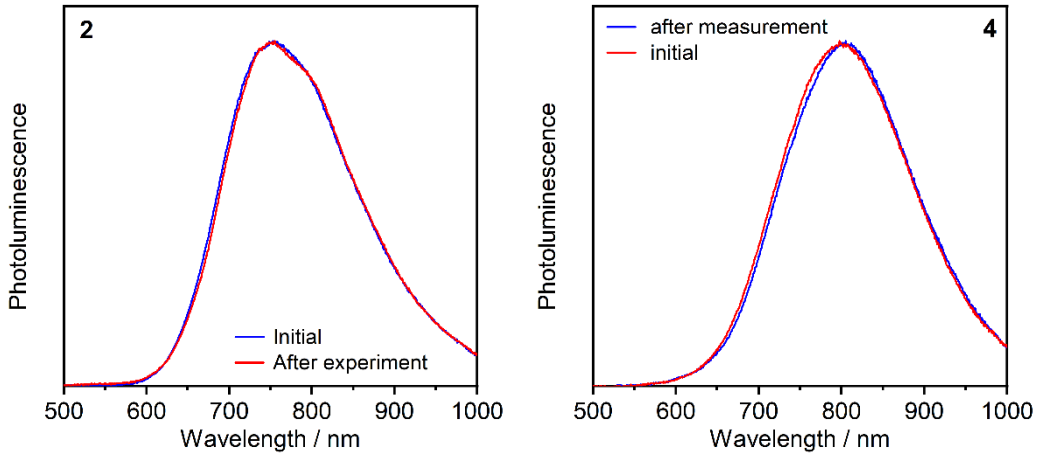

Figure S5.17. Normalised photoluminescence spectra of complexes **2** and **4** in evaporated films obtained before and after the variable-temperature experiments.

Table S5.3. Photoluminescence decay lifetime of complexes **2** and **4** in vacuum-deposited films.

T, K	**2** (770 nm)			**4** (800 nm)		
	τ_1 / µs	**τ_2 / µs**	**τ_{av} / µs**	**τ_1 / µs**	**τ_2 / µs**	**τ_{av} / µs**
300	0.05	0.16	0.12	-	0.11	0.11
250	0.06	0.25	0.21	0.09	0.18	0.15
200	0.10	0.43	0.37	0.09	0.22	0.19
150	0.16	0.65	0.59	0.08	0.27	0.24
110	0.30	0.97	0.87	0.09	0.33	0.30
80	0.42	1.39	1.26	0.09	0.40	0.37

6. Electrochemistry

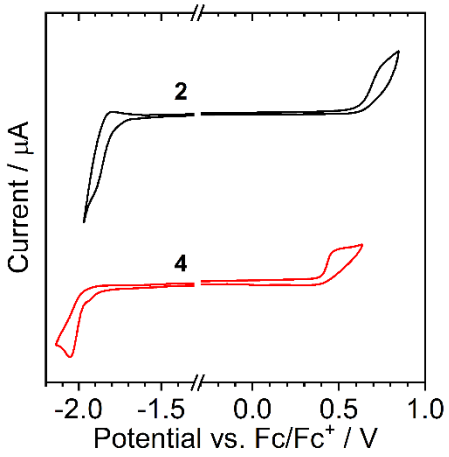

Figure S6.1 Cyclic voltammograms (CV) of **2** (black line) and **4** (red line) at c = 10^{-3} M in 0.1 M Bu_4NBF_4 / CH_2Cl_2 solution.

Table S6.1. Electrochemical onset redox potentials of complexes **2** and **4** recorded in 0.1 M Bu_4NBF_4 / CH_2Cl_2 solution at c = 10^{-3} M.

Complex	**E_{ox} / V**	**E_{red} / V**	**HOMO / eV**	**LUMO / eV**
2	0.63	–1.80	5.73	3.30
4	0.40	–1.96	5.50	3.14

7. OLED devices

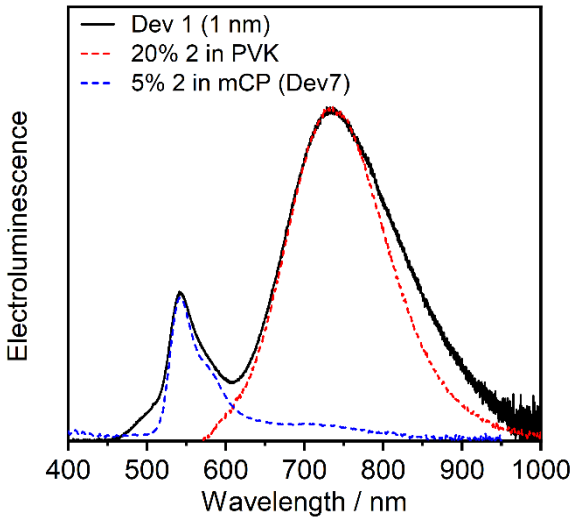

Figure S7.1. Deconvolution of electroluminescence spectrum of Device 1.
Device 7 structure: ITO | HATCN (10 nm) | TSBPA (30 nm) | mCP (5 nm) | mCP co **2** (5 %) (20 nm) | TPBi (40 nm) | PO-T2T (10 nm) | LiF (0.8 nm) | Al (100 nm).

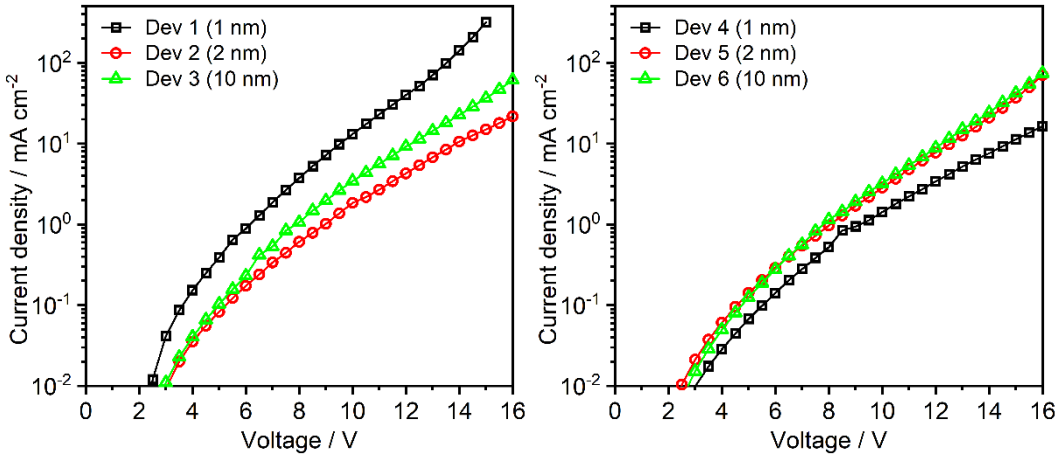

Figure S7.2. Current density-voltage (J-V) characteristics of Devices 1-6.

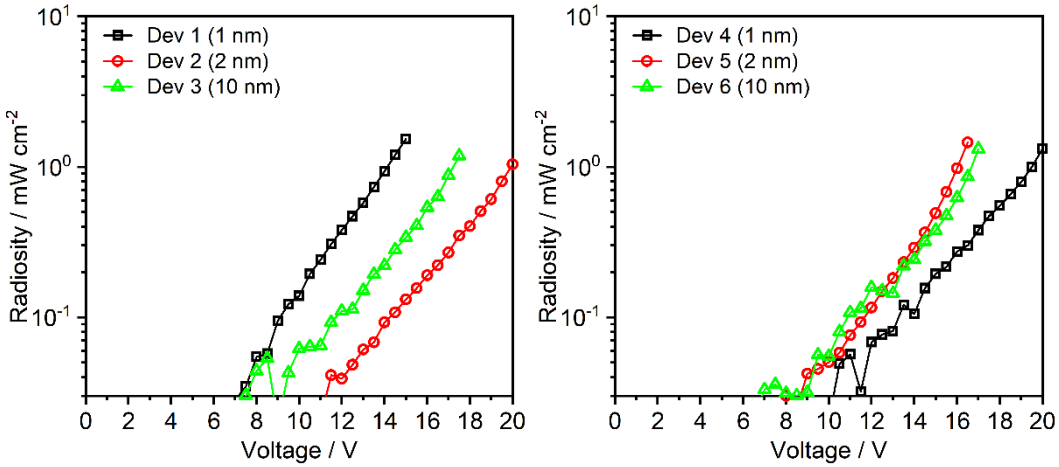

Figure S7.3. Radiosity-voltage characteristics of Devices 1-6.

8. Excimer kinetics in monometallic complexes

Monomer and excimer decay can be described by differential equations (S8.1) and (S8.2), respectively:

$$\frac{dM^*}{dt} = -\left(k_M + k_Q[M]\right)M^* \quad \text{(S8.1)}$$

$$\frac{dE^*}{dt} = k_Q[M]M^* - k_E E^* \quad \text{(S8.2)}$$

Solving equation (S8.1) gives:

$$M^*(t) = Ae^{-\left(k_M + k_Q[M]\right)t} \quad \text{(S8.3)}$$

The Stern-Volmer relation used in the main text can be derived from equation (S8.3):

$$\frac{1}{\tau_M} = \frac{1}{\tau_0} + k_Q[M] \quad \text{(S8.4)}$$

Where τ_M is the monomer emission lifetime at given concentration [M]. $\tau_0 = k_M^{-1}$ is the lifetime of the monomer emission at [M]→0. k_Q is the self-quenching constant, M^{-1} s^{-1}. M* and E* represent concentrations of excited state monomer and excimer species, respectively.

From equation (S8.2) in steady-state conditions equation (S8.5) is obtained.

$$\frac{E^*}{M^*} = \frac{k_Q}{k_E}[M] \quad \text{(S8.5)}$$

Solving equation (S8.2) gives:

$$E^*(t) = A_1 e^{-\left(k_M + k_Q[M]\right)t} + A_2 e^{-k_E t} \quad \text{(S8.6)}$$

In order to satisfy boundary condition E*(t)=0 the A_1=-A_2. While A_1 has a defined value (below) the A_2 is a new constant (constant of integration). Thus, the sign of A_1 will determine the sign of A_2 to be opposite.

$$A_1 = A\frac{k_Q[M]}{k_E - k_Q[M] - k_M} \quad \text{(S8.7)}$$

Equation (S8.7) will have two cases:

$$\begin{aligned} A_1 > 0 \; for \;\; k_E > k_Q[M] + k_M \\ A_1 < 0 \; for \;\; k_E < k_Q[M] + k_M \end{aligned} \quad \text{(S8.8)}$$

From the abovementioned conditions it can be concluded that for excimer decay rates faster than that of the monomer the τ_1 and τ_2 in equation 4 (main text) represent exciton and excimer decay, respectively. Once the monomer decays faster than excimer, the order of constants switches and now τ_1 and τ_2 are excimer and exciton decay, respectively.

9. References

[1] F. Neese, *WIREs Comput. Mol. Sci.* **2018**, *8:e1327*, DOI: 10.1002/wcms.1327.

[2] F. Neese, *WIREs Comput. Mol. Sci.* **2012**, *2*, 73.

[3] S. Lehtola, C. Steigemann, M. J. T. Oliveira, M. A. L. Marques, *SoftwareX* **2018**, *7*, 1.

[4] A.-R. Allouche, *J. Comput. Chem.* **2011**, *32*, 174.

[5] A. D. Becke, *J. Chem. Phys.* **1993**, *98*, 5648.

[6] P. J. Stephens, F. J. Devlin, C. F. Chabalowski, M. J. Frisch, *J. Phys. Chem.* **1994**, *98*, 11623.

[7] F. Weigend, R. Ahlrichs, *Phys. Chem. Chem. Phys.* **2005**, *7*, 3297.

[8] A. D. Becke, *Phys. Rev. A* **1988**, *38*, 3098.

[9] A. Hellweg, C. Hättig, S. Höfener, W. Klopper, *Theor. Chem. Acc.* **2007**, *117*, 587.

[10] F. Weigend, *Phys. Chem. Chem. Phys.* **2006**, *8*, 1057.

[11] F. Neese, F. Wennmohs, A. Hansen, U. Becker, *Chem. Phys.* **2009**, *356*, 98.

[12] R. Izsák, F. Neese, *J. Chem. Phys.* **2011**, *135*, 144105.

[13] S. Grimme, S. Ehrlich, L. Goerigk, *J. Comput. Chem.* **2011**, *32*, 1456.

[14] S. Grimme, J. Antony, S. Ehrlich, H. Krieg, *J. Chem. Phys.* **2010**, *132*, 154104.

[15] P. Data, P. Pander, M. Lapkowski, A. Swist, J. Soloducho, R. R. Reghu, J. V. Grazulevicius, *Electrochim. Acta* **2014**, *128*, 430.

[16] P. Pander, P. Data, R. Turczyn, M. Lapkowski, A. Swist, J. Soloducho, A. P. Monkman, *Electrochim. Acta* **2016**, *210*, 773.

[17] C. M. Cardona, W. Li, A. E. Kaifer, D. Stockdale, G. C. Bazan, *Adv. Mater.* **2011**, *23*, 2367.

[18] J.-L. Bredas, *Mater. Horiz.* **2014**, *1*, 17.

[19] D. de Sa Pereira, A. P. Monkman, P. Data, *J. Vis. Exp.* **2018**, DOI: 10.3791/56593.

[20] D. J. Cárdenas, A. M. Echavarren, M. C. Ramírez de Arellano, *Organometallics* **1999**, *18*, 3337.

[21] Z. Wang, E. Turner, V. Mahoney, S. Madakuni, T. Groy, J. Li, *Inorg. Chem.* **2010**, *49*, 11276.

[22] J.-Y. Lallemand, J. Soulié, J.-C. Chottard, *J. Chem. Soc., Chem. Commun.* **1980**, 436.

[23] O. V. Dolomanov, L. J. Bourhis, R. J. Gildea, J. A. K. Howard, H. Puschmann, *J. Appl. Crystallogr.* **2009**, *42*, 339.

[24] G. M. Sheldrick, *Acta Crystallogr. Sect. A Found. Crystallogr.* **2008**, *64*, 112.

[25] P. Pander, A. V. Zaytsev, A. Sil, J. A. G. Williams, P.-H. Lanoe, V. N. Kozhevnikov, F. B. Dias, *J. Mater. Chem. C* **2021**, *9*, 10276.

[26] J. A. G. Williams, *Chem. Soc. Rev.* **2009**, *38*, 1783.

[27] K. Suzuki, A. Kobayashi, S. Kaneko, K. Takehira, T. Yoshihara, H. Ishida, Y. Shiina, S. Oishi, S. Tobita, *Phys. Chem. Chem. Phys.* **2009**, *11*, 9850.